Models for the amorphization of compressed crystals

1996 J. Phys.: Condens. Matter 8 10907

(http://iopscience.iop.org/0953-8984/8/50/017)

J. Phys.: Condens. Matter **8** (1996) 10907–10918. Printed in the UK

Models for the amorphization of compressed crystals

Robin J Speedy

Chemistry Department, Victoria University of Wellington, PO Box 600, Wellington, New Zealand

Received 21 May 1996, in final form 9 October 1996

Abstract. A permanently bonded diamond network, with flexible bond lengths and angles, is characterized by computer simulation and used as the reference state for a perturbation treatment that favours tetrahedral bond angles. At low temperatures the perturbed system has three phases separated by two sets of van der Waals loops. The intermediate-pressure phase is an open crystal which, like ice or quartz, expands when cooled and collapses under pressure to an amorphous solid. Two-dimensional honeycomb networks show the same behaviour.

1. Introduction

Some crystals collapse sharply to an amorphous solid when they are compressed. Examples are ice [1–3], α quartz (SiO_2) [4], coesite (SiO_2) [4], perovskite ($CaSiO_2$) [5], α berlinite ($AlPO_4$) [6] and aqueous clathrates [7]. Stishovite, a polymorph of silica that is stable at high pressure, becomes amorphous when decompressed [8]. The crystal-to-glass transitions occur at low temperatures where both phases are metastable but where formation of the more stable crystal is slow. The collapse has been studied by computer simulation [9–14] and theoretically [15] with most interpretations focusing on the failure of the Born criteria for mechanical stability. Sciortino *et al* [14] show that when ice is simulated under conditions of extreme compression or tension the compressibility becomes very large and its density dependence suggests spinodal-like divergences near the practical limit of stability of the crystal. Memory effects are reported [6, 7, 10, 13]. For instance, when aqueous clathrates are made amorphous by compression they revert back to the original crystal on decompression [7]. Low-density amorphous solid forms of water [3] and silica [16] also collapse to higher-density amorphous forms when compressed.

Several crystals, including those with a diamond-lattice structure, expand when they are cooled towards absolute zero. Examples are ice ($T < 65$ K), diamond ($T < 90$ K), silicon ($T < 120$ K) and germanium ($T < 48$ K) [17]. Amorphous materials that expand when cooled include glassy silica ($T < 30$ K), other mixed silica-based glasses [17] and the liquids water, silica and silicon. The examples given suggest connections between expansion on cooling, collapse on compression, spinodal instabilities and a preference for tetrahedral bond angles.

This paper develops a model for the above anomalies and suggests that they have a common origin, which may be independent of whether the phases involved are crystalline or amorphous, or even solid. In a tetravalent network, the four bonded neighbours of each particle are as far apart as possible when they are arranged tetrahedrally, so repulsive forces between the non-bonded second neighbours naturally favour the tetrahedral bond angles that occur in diamond lattices. Any variation in the bond angles in a diamond lattice increases

0953-8984/96/5010907+12$19.50

its density, unless there is a compensating increase in the bond lengths, so increasing fluctuations in the bond angles at higher temperatures contribute to a contraction on warming. The collapse under pressure can also occur by varying the bond angles, without breaking bonds. That explains why the collapse can occur readily at low temperatures, where the bond breaking rate is slow, and it can also explain the memory effects [6, 7, 10, 13] because the network topology of the original crystal is stored in the collapsed product.

The first step is to show that a model network, with flexible bond angles and lengths, transforms from an open crystal under tension to dense amorphous forms under compression, without breaking any bonds. This model is later used as the reference system for a perturbation treatment in which the perturbing potential favours tetrahedral bond angles. Most of the perturbed models studied contain two sets of van der Waals loops separating three phases. The phase transitions arise because in the flexible reference system the bond angles can have a broad distribution, but the perturbation can cause the angles to 'condense' to a narrow distribution, analogous to the gas-to-liquid condensation in van der Waals theory. The phase that is stablized by the perturbation models an ice like crystal that expands when cooled and collapses when compressed. It is bounded by spinodal instabilities, consistent with the observations of Sciortino *et al* [14]. The same phenomenology is obtained in two and three dimensions and is insensitive to variation of the only free parameter in the model.

A variety of lattice models [18–21] have been developed to mimic the anomalies of cold water. The advantage of lattice models is that they can be solved analytically to obtain the phase diagram and thermodynamic properties, with well defined approximations, and they show the relation between phase transitions, spinodal line and the loci of density extrema [18–21]. The present approach generates a similar phenomenology from an off-lattice model that, like the examples mentioned above, can become structurally amorphous.

2. Permanently bonded networks

Most papers [9–14] on the simulation of crystal collapse stress the importance of using a potential that accurately represents the properties of a particular real material. This work attempts to capture the generic features that tetravalent network materials have in common rather than the particulars that make them different. It provides a simple model than can reproduce the phenomenology and which may isolate the factors that are essential to its explanation.

A saturated-square-well (SSW) potential [2] is used to model permanently bonded network structures with flexible bond lengths and angles. The topology of the network is that of the trivalent ($N_v = 3$) honeycomb crystal in two dimensions ($D = 2$), as shown in figure 1, or the tetravalent ($N_v = 4$) diamond crystal in three dimensions ($D = 3$). The particles have a hard-sphere core of diameter σ and a square well of diameter $\lambda\sigma$. The rules that define the system are (i) the bonds present in the starting configuration (honeycomb or diamond lattice) cannot break and no other bonds can form, (ii) the separation between the centres of bonded pairs is always in the range σ–$\lambda\sigma$ and (iii) the separation between non-bonded pairs is always greater than $\lambda\sigma$. The honeycomb lattice was modelled by the SSW ($N_v = 3$, $D = 2$) potential with $\lambda = 1.3$, 1.4, 1.5 and $\sqrt{3}$ and the diamond lattice by the SSW ($N_v = 4$, $D = 3$) potential with $\lambda = 1.2$, 1.3, 1.4, 1.5 and $\sqrt{(8/3)}$. Most of the simulations were for $N = 512$ ($D = 3$) or $N = 600$ ($D = 2$) particles in a cubic ($D = 3$) or rhomboidal ($D = 2$) cell with periodic boundaries, using the molecular dynamics technique pioneered by Alder and Wainwright [23]. The above rules were implemented by forcing a pair to bounce elastically whenever their separation reached σ or $\lambda\sigma$. The dynamics of a bounce are determined by the conversation of energy and linear momentum and by the fact

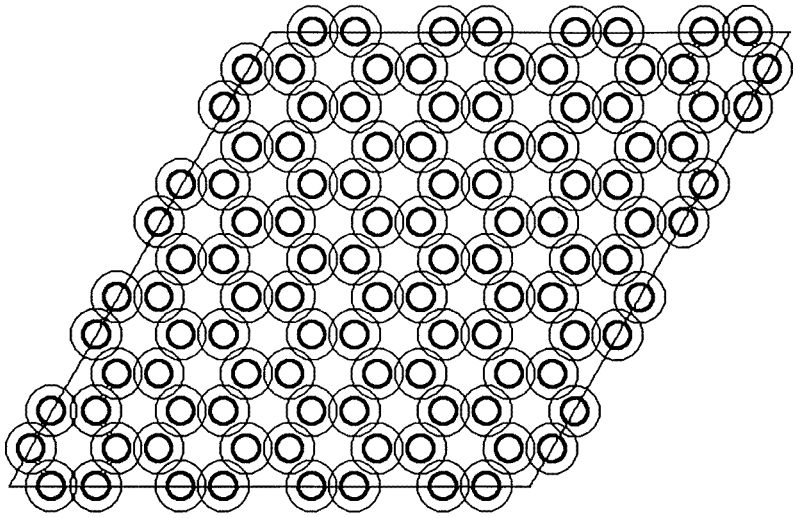

Figure 1. The honeycomb lattice starting configuration for $N = 96$ SSW ($N_v = 3$, $D = 2$, $\lambda = \sqrt{3}$) particles. Small circles of diameter σ show the hard cores and larger circles of diameter $\lambda\sigma$ show the square well. Particles are bonded when their larger circles overlap. Non-bonded particles bounce like hard spheres of diameter $\lambda\sigma$.

that the impulse is transmitted along the line of the centres of the bouncing pair.

The density scale, $z = \sqrt{27}(N/V)(\sigma/2)^D$, is chosen such that $z = 1$ in the perfect crystal when all bonded pairs are at the contact separation σ and all bond angles are equal. z can exceed unity when λ is small because the crystals can deform to denser structures by varying the bond angles, as shown in figure 2. There is a special value of $\lambda(\lambda = \sqrt{3}$ when $D = 2$ [22] and $\lambda = \sqrt{(8/3)}$ when $D = 3$ [24]) for which the closest-packed state is a perfect honeycomb or diamond crystal with $z = 1$ and non-bonded second neighbours are in contact at the separation $\lambda\sigma$. These models have been studied previously [22, 24, 25].

Figure 3 shows how the pressure varies with density. The permanently bonded networks can be stretched to the limit where the bond lengths are at their maximum extension $\lambda\sigma$. In this limit they are perfect honeycomb or diamond crystals, the density is $z = \lambda^{-D}$ and the pressure diverges to minus infinity. The pressure divergence was found empirically to have the form

$$PV/Nk_BT = C_1/(1 - \lambda^D z) \tag{1}$$

with $C_1 = 1.76$ ($D = 2$) and $C_1 = 2.56$ ($D = 3$). P is the pressure, V is the volume (area) of the simulation cell and k_BT is Boltzmann's constant multiplied by the temperature. At large tensions (negative pressures), core collisions between bonded pairs are rare so all the models have the same PV/Nk_BT at the same value of the scaled density, $\lambda^D z$. Equation (1) reproduces pressures measured in the range $-10 > PV/Nk_BT > -100$ to within 1%, except for the case $\lambda = 1.2$ where core collisions between bonded pairs remain significant to $PV/Nk_BT = -20$. In the high-density extreme the pressure diverges to plus infinity at a density z_{max} with the form [22, 24, 25]

$$PV/Nk_BT = C_2/(1 - z/z_{max}). \tag{2}$$

When the close-packed state is crystalline $C_2 = D$ but when it is amorphous $C_2 < D$ [24, 25]. In the intermediate-pressure range $-10 < PV/Nk_BT < 20$, where equations (1)

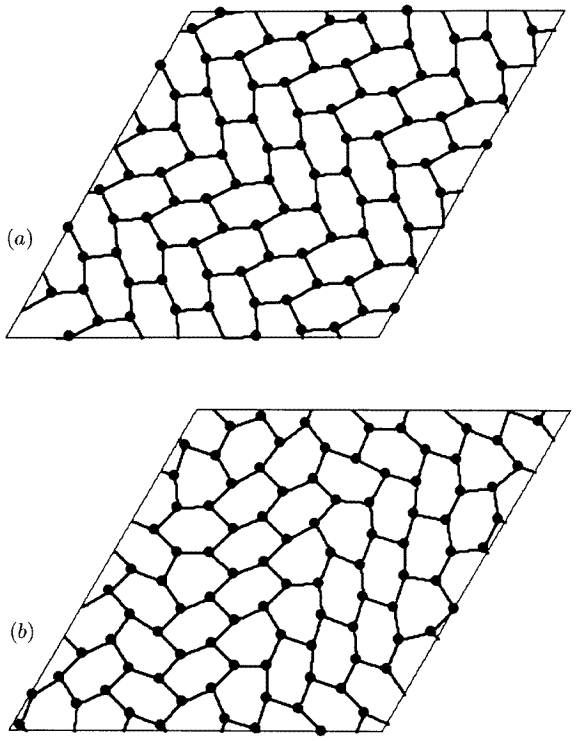

Figure 2. Two high-density configurations of $N = 96$ SSW ($N_v = 3$, $D = 2$, $\lambda = 1.4$) permanently bonded particles. Dots locate the particle centres and lines show the bonds. (*a*) A crystalline structure at density $z = 1.1$ where $PV/Nk_BT = 157.4$. The radial and angle distribution functions for this structure show sharp peaks. (*b*) A glassy structure at density $z = 1.08$ where $PV/Nk_BT = 165.5$. Radial and angle distribution functions for this structure show broad peaks.

and (2) are inaccurate, the measured pressures were fitted to four- or five-degree polynomials in density for use in the following perturbation treatment.

Small systems were studied to check for size effects, which might be important if ordered states are forced to accommodate a simulation cell that does not match their structure. For instance, the honeycomb and diamond lattices can both be compressed anisotropically to 'brick wall' structures that fit a rectangular cell. Sciortino *et al* [14] simulated ice at constant density in a cubic cell of fixed shape and at constant pressure in a cell of flexible shape and found only small differences in the equation of state and the pressure where the ice collapsed. Two-dimensional networks with $N = 96$ and $1.3 \leqslant \lambda \leqslant 1.5$ show a weak, reversible, first-order phase transition in which the density changes by 1–2%. The structural origin of the transition is shown in figure 2. The lower-density phase has a disordered glassy structure, somewhat like a Penrose tiling with several different tile shapes, and the higher-density phase is an ordered crystal in which all the hexagons have the same bricklike shape. Formation of the crystalline structure is slow and it can be avoided by compressing rapidly to high density. For the larger systems of $N > 500$ particles that were used in the quantitative analyses the high-density crystalline form was not observed and the high-density state was a disordered glass when $\lambda \leqslant 1.5$, as shown in figure 4. The radial distribution functions for three-dimensional crystalline and amorphous structures near their close-packed limits are

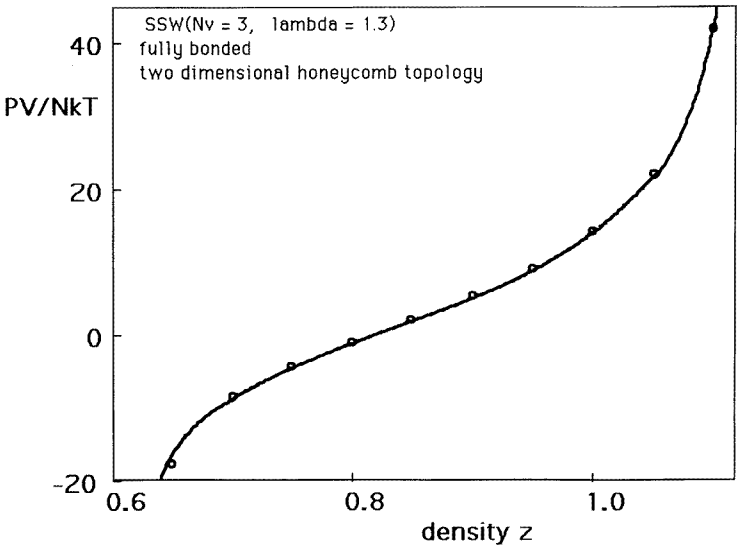

Figure 3. The pressure, PV/Nk_BT, for $N = 600$ SSW ($N_v = 3$, $D = 2$, $\lambda = 1.3$) permanently bonded particles versus density. The line shows equation (2) (with $C_2 = 1.87$ and $z_{max} = 1.15$) when $z \geqslant 1.05$, equation (1) when $z \leqslant 0.7$ and a polynomial fit for $0.7 < z < 1.05$.

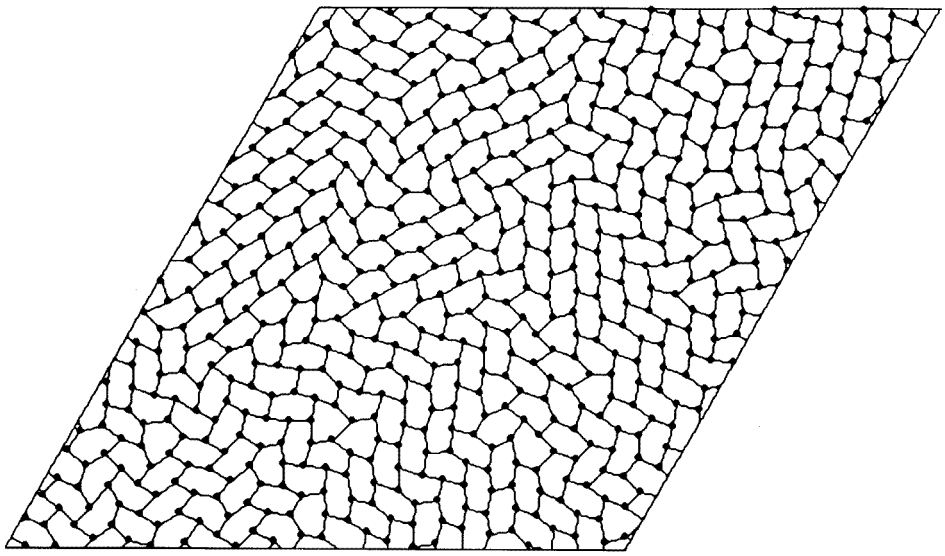

Figure 4. A disordered configuration of $N = 600$ SSW ($N_v = 3$, $D = 2$, $\lambda = 1.3$) permanently bonded particles at the highest pressure shown in figure 3. Dots locate the particle centres and lines show the bonds. The radial distribution function for this structure is close to unity beyond three diameters.

compared in figure 5.

The main conclusion to be drawn from figures 4 and 5 is that the open crystalline networks that are stable under tension can transform under pressure to dense amorphs which

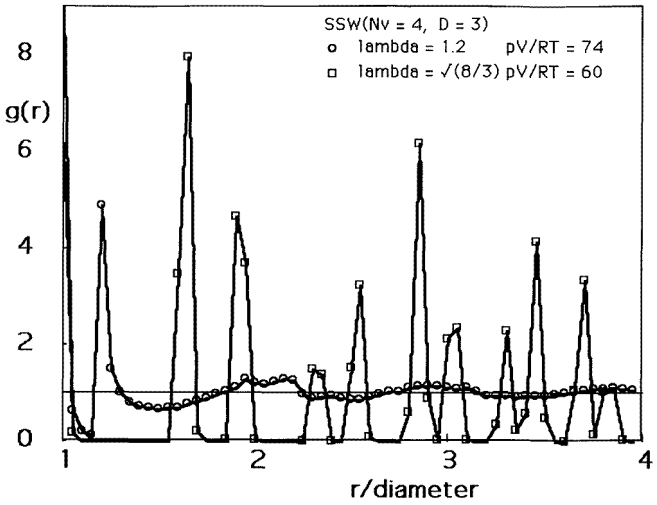

Figure 5. The radial distribution function $g(r)$ versus r/σ for a crystalline structure of the SSW ($N_v = 4$, $D = 3$, $\lambda = \sqrt{(8/3)}$) model at density $z = 0.95$ where $PV/Nk_BT = 59.62$ and for an amorphous structure of the fully bonded SSW ($N_v = 4$, $D = 3$, $\lambda = 1.2$) model at density $z = 1.35$ where $PV/Nk_BT = 74$. The points are from course-grained averages over spherical shells of volume $4\pi r^2\,\delta r$, with a thickness $\delta r = \sigma/20$, and straight lines are drawn between successive points to guide the eye.

have the same network topology as the crystal but do not have long-range geometrical order. Except for the crystallization of small systems mentioned in the previous paragraph, there is no indication of any discontinuity in the pressure between the high- and low-density limits, but first-order discontinuities emerge when the model is augmented by a potential that stabilizes the open bond angles of the low-density crystal.

3. Perturbation treatment

The effect of adding an angle dependent potential is estimated here from a perturbation treatment. The logic follows earlier perturbation theories for fluids [26, 27] but uses a different reference system and a different perturbing potential. The models described in the previous section provide the reference system and the perturbing potential is applied to the bond angles.

To simplify the equations the configuration integral for the reference system is expressed as a sum over $k = 1, 2, \ldots, \Omega$ discrete configurations. This can be accomplished by imagining the space of volume V to be subdivided into a lattice of V/ω very small cells, each of volume ω. Space is 'quantized' in this way by the finite number of significant figures used to represent the particle positions in simulations, for example. A configuration can then be specified by a list of the N cells where the particle centres are located. In each one of those configurations each particle centre can move over the volume ω of its cell so each configuration contributes ω^N to the configuration integral. The potential energy of the reference system is taken to be zero and its configuration integral can be expressed as

$$Q_0(N, V, T) = \omega^N \Omega(N, V, \omega) \tag{3}$$

where the subscript zero is used to indicate a property of the reference system.

The energy $u(\theta)$ associated with the bond angle θ between a pair of bonds that meet at a common vertex is arbitrarily assigned the simple harmonic form

$$u(\theta) = E(\theta - \theta_T)^2 \tag{4}$$

where θ_T is the angle where the energy is a minimum and E is an energy which specifies the strength of the perturbation. In this work $\theta_T = 120^\circ$ in two dimensions and the tetrahedral angle 109.47° in three dimensions. Repulsions between non-bonded second neighbours will favour structures with $\theta = \theta_T$ because the second neighbours are then as far apart from each other as possible.

When the perturbation is turned on the potential energy of configuration k is

$$U_k = n_b N E \langle(\theta - \theta_T)^2\rangle_k \tag{5}$$

where $\langle(\theta - \theta_T)^2\rangle_k$ is an average over all the bond angles in configuration k and $n_b = N_v(N_v - 1)/2$ is the number of bond angles per molecule. The potential energy of configuration k is expressed in terms of its fluctuation from the mean value

$$U_k = \langle U_k\rangle_0 + \Delta U_k \tag{6}$$

where $\langle U_k\rangle_0 = n_b N E \langle\langle(\theta - \theta_T)^2\rangle_k\rangle_0$ is an average over the configurations of the reference system. The perturbed system samples the same set of $\Omega(N, V, \omega)$ configurations as the reference system and its configuration integral is therefore

$$Q = \sum_{k=1}^{\Omega} \omega^N \exp\{-\beta U_k\} = Q_0 \exp\{-\beta\langle U_k\rangle_0\}\langle\exp\{-\beta\,\Delta U_k\}\rangle_0 \tag{7}$$

where $\beta = (k_B T)^{-1}$.

To calculate the last average in equation (7), $\langle\exp\{-\beta\,\Delta U_k\rangle_0$, the distribution of the fluctuations in the reference system is assumed to be Gaussian [26, 27] so that, with the abbreviations $x = \Delta U_k$ and $a = (2\langle x_0^2\rangle)^{-1}$,

$$p(x)\,\mathrm{d}x = \sqrt{(a/\pi)}\exp\{-ax^2\}\,\mathrm{d}x. \tag{8}$$

The Gaussian form neglects any higher moments of the distribution and truncates the perturbation expansion at second order. It yields

$$\langle\exp\{-\beta\,\Delta U_k\}\rangle_0 = \int_{-\infty}^{+\infty} p(x)\exp\{-\beta x\}\,\mathrm{d}x = \exp\{\beta^2\langle(\Delta U_k)^2\rangle_0/2\}. \tag{9}$$

Equations (7) and (9) give the configuration integral of the perturbed system in terms of averages that can be measured in the reference system. The configurational part of the Helmholtz potential, $A = -k_B T \ln\{Q\}$, is

$$A = A_0 + \langle U_k\rangle_0 - 0.5\beta\langle(\Delta U_k)^2\rangle_0 \tag{10}$$

and the pressure $P = -(\partial A/\partial V)_T$ is given by

$$PV/Nk_BT = P_0V/Nk_BT + n_b z(E/k_BT)(\mathrm{d}f_1/\mathrm{d}z)_0 - 0.5(n_b z E/k_BT)^2(\mathrm{d}f_2/\mathrm{d}z)_0 \tag{11}$$

where f_1 and f_2 are abbreviations for the averages $f_1 = \langle\langle(\theta - \theta_T)^2\rangle_k\rangle_0$ and $f_2 = N\langle[\langle(\theta - \theta_T)^2\rangle_k - f_1]^2\rangle_0$.

During the simulations reported in the previous section f_1 and f_2 were averaged over 100–500 configurations of 512 or 600 particles during runs of one to two million collisions. The second-order term f_2 is generally much smaller than the first-order term f_1 as shown in figure 6. No attempt was made to compute higher-order terms because f_2 is already very small and shows a scatter of 5–10%. The results were fitted to empirical polynomials in the variable $(z_{max} - z)(z - \lambda^{-D})$ to estimate the density derivatives required in equation (11),

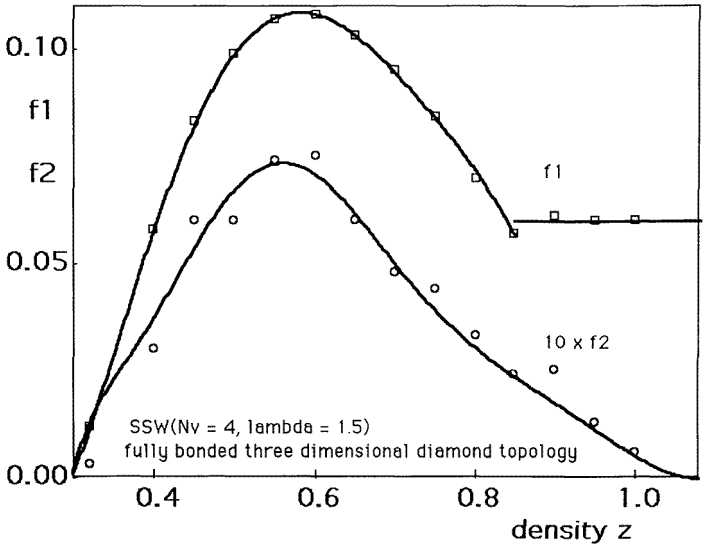

Figure 6. The fluctuation terms f_1 and f_2 (defined after equation (11)) versus density for a three-dimensional system of $N = 512$ SSW ($N_v = 4$, $D = 3$, $\lambda = 1.5$) permanently bonded particles. f_2 is amplified by a factor of ten. The curves are polynomials in $(z_{max} - z)(z - \lambda^{-D})$ that fit f_1 to within ± 0.0015 ($z \leqslant 0.85$) and f_2 to within ± 0.0006. At densities above $z = 0.85$ f_1 becomes independent of density and the following perturbation analyses were applied only in the lower-density range where f_1 varies smoothly with density. The maxima in f_1 and f_2 occur near the density where the pressure is zero in all the models.

When the high-density state is amorphous f_1 becomes constant before the high-density limit is reached, suggesting that the bond angle fluctuations becomes frozen in. The following perturbation analyses are limited to the lower-density region where f_1 varies smoothly with density, to avoid any complication from the apparent discontinuity in the slope $(\mathrm{d}f_1/\mathrm{d}z)_0$.

4. Results

Figure 7 shows pressure–volume isotherms calculated from equation (11) for the two-dimensional model with $\lambda = 1.3$. This is the model whose high-density structure is shown in figure 4. Features of figure 7 are the emergence of two sets of van der Waals loops and an intermediate phase that expands when cooled at high pressure before collapsing to a denser phase. These features are common to the two-dimensional models with $\lambda = 1.3$ and 1.4 and the three dimensional models with $\lambda = 1.2$, 1.3, 1.5 and $\sqrt{(8/3)}$. The maxima and minima on the isotherms in figure 7 locate the spinodal lines, where the compressibility diverges, and Maxwell's equal-area construction gives the phase coexistence lines, which are shown in the pressure–temperature phase diagram (figure 8). For the negative-pressure loops the critical temperature is near $k_BT/E = 1/6$ for all the models, the critical pressures are in the range $PV_0/NE = -2 \pm 1.5$ and the slope of the coexistence line in figure 8 is positive, $\mathrm{d}p_{trans}/\mathrm{d}T > 0$, which shows that the perturbing potential favours the intermediate phase in the density range of the low-pressure transition. For the positive-pressure loops the critical temperature for the different models is in the range $1/6 > k_BT/E > 1/8$, the critical pressures are in the range $1 < PV_0/NE < 15$ and $\mathrm{d}P_{trans}/\mathrm{d}T < 0$, which indicates

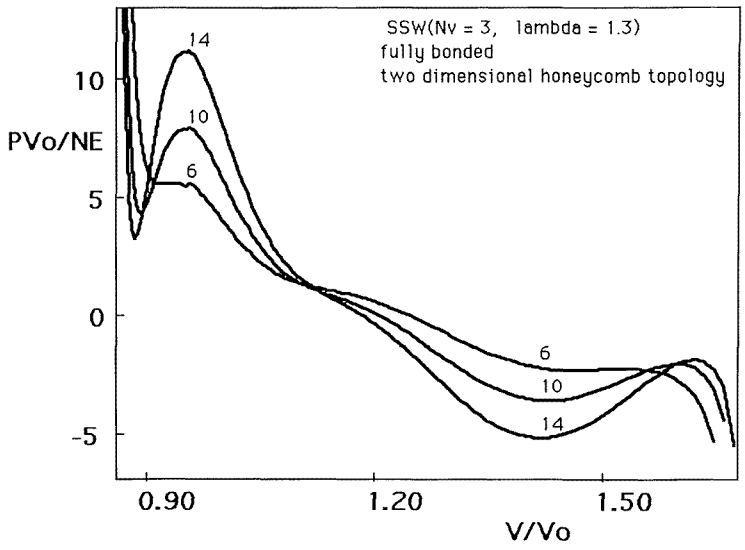

Figure 7. The pressure, PV_0/NE, predicted by equation (11) for the perturbed SSW ($N_v = 3$, $D = 2$, $\lambda = 1.3$) model versus the volume ($V/V_0 = 1/z$). Numbers show the value of E/k_BT.

that the perturbing potential also favours the intermediate phase relative to the high-density phase. The intermediate phase models an icelike crystal which is energetically stabilized by minimizing the variation of the bond angles from θ_T. When $\lambda \leqslant 1.5$ the dense state is a glassy material like than shown in figure 4, so the high-pressure transition corresponds to the collapse of an icelike crystal to an amorphous solid without breaking any bonds. The collapse also occurs in the special cases where the densest state is a perfect crystal.

The two-dimensional model with $\lambda = \sqrt{3}$ shows only the high-pressure loops. The other two models studies ($\lambda = 1.4$, $D = 3$ and $\lambda = 1.5$, $D = 2$) revealed only the negative-pressure loops but in these cases the variance in the bond angles f_1, in the reference system, becomes constant at a relatively low pressure and the perturbation analysis was not applied in the higher-density range where the location of the high-pressure loops is suggested by interpolation from the other models.

The models expand when they are cooled near the high-pressure end of the intermediate phase. The expansivity $\alpha = (\partial \ln\{V\}/\partial T)_p$ is related to the thermal pressure coefficient $\gamma = (\partial P/\partial T)_V$ and the compressibility $\kappa = -(\partial \ln\{V\}/\partial P)_T$ by $\alpha = \kappa\gamma$. Since κ is positive for stable or metastable states, α has the same sign as γ, so where the pressure increases as E/k_BT is increased, at a constant volume (figure 7), the expansivity is negative.

Where two pressure–volume isotherms intersect, $\alpha = \gamma = 0$ and the density is an extremum on an isobar. At low temperatures the pressure–volume isotherms shown in figure 7 (and for all the other models that show both loops) cross at a common volume where the pressure is close to zero, which means that the locus of the density maximum is approximately isochoric and isobaric. This result has a simple explanation in terms of the relation

$$\gamma = P_0/T - (2k_BT^2)^{-1}N(n_bE)^2(\mathrm{d}f_2/\mathrm{d}V)_0 \tag{12}$$

which is obtained by differentiating equation (11) and noting that, in the reference system, $\gamma_0 = (\partial P_0/\partial T)_V = P_0/T$. When the reference system is at the density where its pressure,

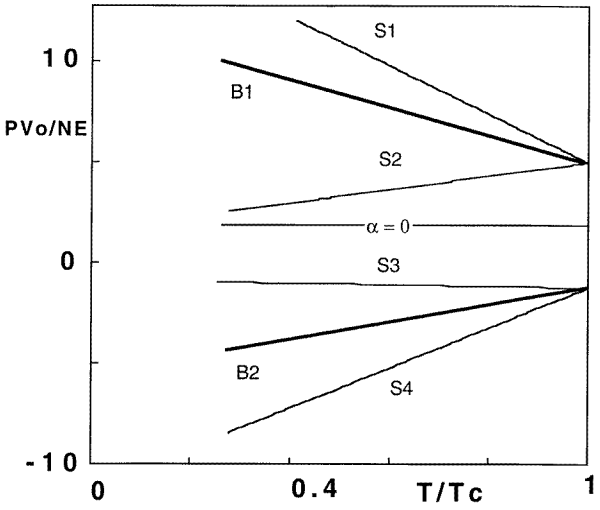

Figure 8. Qualitative sketch of the phase boundaries, spinodal lines and locus of the density maximum in the pressure–temperature plane for the perturbed SSW ($N_v = 3$, $D = 2$, $\lambda = 1.3$) model. B1 and B2 are the binodal lines, where two phases are in equibibrium, estimated by drawing Maxwell equal-area constructions across the loops shown in figure 7. S1–S4 are the spinodal lines, which are the loci of pressure extrema on the isotherms in figure 7. S1 and S4 are the limits of stability of the intermediate phase under compression and tension, respectively. $\alpha = 0$ shows the locus of the density maximum. All the models that show two sets of van der Waals loops yield a qualitatively similar diagram. For the model shown the critical temperature is near $k_BT/E = 1/6$ for both transitions so the ordinate is $T/T_c = 6/(E/k_BT)$.

P_0, is zero, the bond angles are least constrained by external forces and the fluctuation terms f_1 and f_2 in figure 6 are both near their maxima where $(\mathrm{d}f_1/\mathrm{d}V)_0 = 0$ and $(\mathrm{d}f_2/\mathrm{d}V)_0 = 0$. When this is the case equations (11) and (12) predict that α and γ are zero at the density where $P \approx P_0 = 0$.

The spinodal lines which mark the limits of stability of the icelike phase, shown as S1 and S4 in figure 8, are also nearly isochoric. For example, the spinodal line S1 in figure 8 corresponds to the maxima which occur near the volume $V/V_0 = 1$ in figure 7. Sciortino *et al* [14] made a similar observation for simulated ice and cristobalite. For instance, they found that ice collapses when compressed to a volume of 15.8 $\mathrm{cm}^3\ \mathrm{mol}^{-1}$ and ruptures when stretched to 22.7 $\mathrm{cm}^3\ \mathrm{mol}^{-1}$, despite an order of magnitude variation in the temperature. It is interesting that the latter volume is close to the volume, 22.3 $\mathrm{cm}^3\ \mathrm{mol}^{-1}$ [28], where extrapolations suggest that liquid water becomes unstable near -200 MPa in the 0–50 °C temperature range. A possible implication is that ice and water both become unstable at about the same density when they are stretched [29] to -200 MPa.

The apparent discontinuity in the slope $(\mathrm{d}f_1/\mathrm{d}z)_0$ at high density, shown in figure 6, would generate a third 'loop' in the range of stability of the high-density phase. However, the discontinuity is probably the result of the 'freezing in' of the bond angles and no significance is attached to it here.

Several reservations about the reliability of the perturbation treatment need to be stated. Transitions between phases of different symmetry do not have critical points because the phases cannot become identical. The perturbation treatment is a mean-field approximation which may generate artificial critical points and spinodal lines. In view

of the low temperature needed to reveal the first-order transitions, $k_BT/E \leqslant 1/6$, the accuracy of the second-order perturbation treatment, which neglects terms in $(E/k_BT)^3$ and higher, is suspect. Significant uncertainty in the predicted pressures arises from the numerical calculation of the slopes of the lines shown in figure 6, although the qualitative phenomenology is not changed by using different fitted functions to estimate the slopes. The fixed shape of the simulation cell may influence the properties of the reference state at high density.

Despite these reservations, the models display a common phenomenology which is insensitive to the dimensionality, to the value of λ and to variations in the numerical analyses, and a similar phenomenology is derived, with mean-field approximations, from lattice models for materials that expand when cooled [18–21]. Those similarities give some grounds for supposing that the phenomenology derived from the perturbation analysis is qualitatively correct, in the mean-field approximation, and that it provides a useful guide to the interpretation of experiments and to the development of better models.

5. Conclusions

The calculations show that open-network crystals, stabilized by a potential that favours tetrahedral bond angles, can collapse under pressure, by varying the bond angles, to a denser state that can be amorphous. The collapse also occurs in the models in which the densest state is a perfect crystal, in which case there may be no objection to a scenario that includes a critical point because both phases have the same symmetry. The collapse occurs without breaking bonds so that the dense product stores a memory of the bond topology of the original crystal and is likely to reform the same crystal when decompressed. The limits of stability of the open-network crystals under extreme pressure or tension are spinodal lines where the compressibility diverges.

The model makes the counter-intuitive predictions that near the high-pressure limit of the open crystal the compressibility increases with pressure and the expansivity is negative. A simulation study [14] of ice and cristobalite supports the first of these predictions by showing that the variation of volume with pressure has the form predicted [28] near a mean-field spinodal. Experiment [3] and simulation [9] both show that the pressure where ice collapses decreases as the temperature is increased, which agrees with the negative slopes of the lines S1 and B1 in figure 8. For the spinodal line to have a negative slope the expansivity in its vicinity must be negative [28]. At atmospheric pressure, the density of ice 1h goes through a maximum at 63 K and the expansivity is negative at temperatures below 63 K [17, 30]. If the collapse of ice at high pressure [1–3] is indeed due to a spinodal instability, then the expansivity of ice must be negative at the pressure and temperature of the collapse. The model therefore makes the testable prediction that the density maximum in ice shifts to higher temperatures at high pressure.

Polyamorphism [31, 32], the occurrence of more than one distinct amorphous condensed phase of the same composition but with different density, has not been studied here. The best known example is the transformation of the high-density amorph (HDA) formed by compressing ice [1–3] to a low-density amorph (LDA). When the HDA is recovered at atmospheric pressure and warmed above 117 K it transforms to the LDA with a 20% volume increase [3]. According to the present model the HDA would expand back into the ice form from which it was made because bonds do not break. However, while hydrogen bonding seems to be complete in HDA and LDA water [33], LDA water is less stable than ice and freezes near 150 K with the evolution of about 1300 J mol^{-1} of heat [1–3], which suggests that some reorganization of the bond occurs during the formation of HDA and

LDA water. Some HDA clathrates [7] do regenerate the original crystal on decompression.

Polyamorphism might be studied by starting with a reference system in which the bond patterns are those of an amorphous solid or liquid. Slowly quenched glasses of the SSW ($N_v = 4$, no Δ) model have only 1% of their bonds broken [25] and could be used for the reference system, for instance. While this reference system might differ in some qualitative way from the crystalline one used here, it seems likely that it could generate an analogous polyamorphic phenomenology. Mishima [3] argued that the existence of the HDA and the LDA implies that there are two distinct liquid phases of water and Tanaka has found some evidence for the two liquids in a simulation study [34].

Acknowledgment

I am grateful for support from the Marsden Fund through contract number GRN501.

References

[1] Mishima O, Calvert L D and Whalley E 1984 *Nature* **310** 393
[2] Mishima O, Calvert L D and Whalley E 1985 *Nature* **314** 76
[3] Mishima O 1994 *J. Chem. Phys.* **100** 5910
[4] Hemley R J, Jephcoat A P, Mao H K, Ming L C and Manghnani M H 1988 *Nature* **334** 52
[5] Liu L G and Ringwood A E 1975 *Earth Planet Sci. Lett.* **28** 209
[6] Kruger M B and Jeanloz R 1990 *Science* **249** 647
[7] Handa Y P, Tse J S, Klug D D and Whalley E 1991 *J. Chem. Phys.* **94** 623
[8] Skinner B J and Fahy J J 1963 *J. Geophys. Res.* **68** 5595
[9] Tse J S and Klein M L 1990 *J. Chem. Phys.* **92** 3992
[10] Tse J S 1992 *J. Chem. Phys.* **96** 5482
[11] Tse J S and Klug D D 1991 *J. Chem. Phys.* **95** 9176
[12] Tse J S and Klug D D 1991 *Phys. Rev. Lett.* **67** 3559
[13] Tse J S and Klug D D 1993 *Phys. Rev. Lett.* **70** 174
[14] Sciortino F, Essmann U, Stanley H E, Hemmati M, Shao J, Woolf G H and Angell C A 1995 *Phys. Rev.* E **52** 6484
[15] Binggeli N and Chelikowsky J R 1992 *Phys. Rev. Lett.* **69** 2220
[16] Grimsditch M 1984 *Phys. Rev. Lett.* **52** 2379
[17] Collins J G and White G K 1964 *Prog. Low. Temp. Phys.* **4** 450
[18] Sasai M 1990 *J. Chem. Phys.* **93** 7329
[19] Sastry S, Sciortino F and Stanley H E 1993 *J. Chem. Phys.* **98** 9863
[20] Borick S S, Debenedetti P G and Sastry S 1995 *J. Phys. Chem.* **99** 3781
[21] Roberts C J and Debenedetti P G 1996 *J. Chem. Phys.* **105** 658
[22] Speedy R J 1992 *J. Phys. Chem.* **97** 2723
[23] Alder B J and Wainwright T E 1960 *J. Chem. Phys.* **33** 1439
[24] Speedy R J and Debenedetti P G 1994 *Mol. Phys.* **81** 237
[25] Speedy R J and Debenedetti P G 1996 *Mol. Phys.* **88** 1293
[26] Zwanzig R W 1954 *J. Chem. Phys.* **22** 1420
[27] Barker J A and Henderson D J 1967 *J. Chem. Phys.* **48** 4714
[28] Speedy R J 1982 *J. Phys. Chem.* **86** 982
[29] Henderson S J and Speedy R J 1987 *J. Phys. Chem.* **91** 3069
[30] Dantle G 1962 *Z. Phys.* **166** 115
[31] Angell C A 1995 *Science* **267** 1924
[32] Aasland S and McMillan P F 1994 *Nature* **369** 633
[33] Whalley E, Klug D D and Handa Y P 1989 *Nature* **342** 783
[34] Tanaka H 1996 *Nature* **380** 328